Geophys. J. R. astr. Soc. (1967) **13**, 31–59.

Inhomogeneities in the Earth's Mantle*

M. Nafi Toksöz, Michael A. Chinnery and Don L. Anderson

Summary

Using seismic body and surface waves, the velocity structure of the Earth's mantle is determined with the emphasis on regions of anomalous variations (so-called 'discontinuities'). In the upper mantle, the interpretation of Rayleigh and Love wave dispersion curves yields shear velocity profiles with discontinuities at depths 350 km and 700 km, and a low-velocity zone extending to 350 km. In the lower mantle *P*-velocity profile is determined from $dt/d\Delta$ measurements using large aperture seismic array and travel times from Long Shot nuclear explosion for the Japan–Kuriles–Aleutian–Montana path. The velocity structure shows anomalous gradients or 'discontinuities' at depths 700, 1200 and 1900 km, indicating that the lower mantle is not homogeneous.

Lateral variations of the velocity structures are investigated. For the upper mantle studies the Earth is divided into three regions: oceanic areas, continental shields, and tectonic zones. Pure path phase velocities of Love waves are extracted from the composite dispersion data. The pure path shear velocity profiles obtained from these data are characterized by lower velocities under the oceans in the uppermost portion of the mantle. Shields have the highest velocities. These velocity differences are interpreted in terms of temperature variations. At a depth of 110 km the temperature of the oceanic mantle is higher (by 100–500° C depending on the temperature coefficient of the velocity) than that of the mantle under the shields. The presence of lateral heterogeneities in the mantle is demonstrated qualitatively by the differences of $dt/d\Delta$ vs Δ curves for two separate paths.

Undulations of the geoid as determined from satellite observations are investigated for determining the sources of the anomalies. It is concluded that the main sources of lateral density variations must be in the mantle at depths greater than about 100 km.

1. Introduction

Seismic body and surface wave studies have contributed greatly to our knowledge of the Earth's interior. Early work on the interpretation of travel times of *P* and *S* waves has provided much information about the velocity distribution in the Earth's mantle and core, and on this basis the major divisions such as upper mantle, transition zone and lower mantle have been established. Since the introduction of the Earth models of Gutenberg and Jeffreys, new tools, new data and sophisticated seismic

* Contribution No. 1425, Division of Geological Sciences, California Institute of Technology, Pasadena.

interpretation techniques have become available. Some examples of these are the following:

1. Seismic surface wave dispersion data have been obtained from recordings of long-period instruments. These have been interpreted by computations made feasible with the availability of high-speed computers.

2. Low altitude and subsurface nuclear explosions whose locations and origin times are known precisely have provided travel time data with an accuracy unobtainable from earthquake studies.

3. Large seismic arrays such as LASA and the extended array at Tonto Forest are providing direct measurements not only of travel times but also of the distance derivatives ($dt/d\Delta$, $d^2t/d\Delta^2$) of these times. The derivatives are more sensitive to the velocity structure at depth than are the travel times.

4. Data from sources other than seismology are becoming available for investigation of the Earth's mantle. For example, the distribution of heat flow over the globe, satellite observations of geoid heights, and high pressure and high temperature laboratory experiments are providing information that can be correlated with seismic observations.

In this paper we utilize both old and new data to discuss the structure of the Earth's mantle, with particular regard to evidence for vertical and lateral inhomogeneities. First, we review the seismic methods used and the results of the interpretation of seismic data in investigating anomalous variations in velocity and velocity gradients. Then we discuss lateral variations in mantle structure indicated by seismic surface and body wave results. The last section contains a discussion of the correlation of the seismic data with other geophysical information, and mentions some of the implications of these data on the nature of the mantle.

2. Vertical inhomogeneities or 'discontinuities' in the mantle

The term 'vertical inhomogeneity' or discontinuity will refer to an anomalous variation of seismic velocity with depth which may be characterized by a change in the velocity–depth profile. This may be a discontinuous velocity jump (i.e. first order discontinuity) such as the Mohorovičić discontinuity or a continuous velocity structure that is discontinuous in one of the derivatives of velocity with depth (i.e. second or higher order discontinuity). A chemically homogeneous planet with no solid–solid or solid–liquid phase changes will have a smoothly varying velocity curve. Thus, 'discontinuities' in the velocity–depth curves in the Earth's mantle would represent departures from homogeneity as defined above.

In determining the seismic velocity variation with depth, the travel times of P and S waves and the dispersion of Rayleigh and Love waves, as well as data from free oscillations, can be utilized. The description of pertinent techniques and some results can be found in a number of review papers (Nuttli 1963, Press 1964, and Anderson 1965). In the upper mantle, travel time and body wave studies are complicated by the presence of decreases or rapid changes in velocity, and surface wave techniques have been more successful. For lower mantle studies, however, both surface wave and body wave methods have limited resolving power. A technique utilizing an array of seismometers for the measurement of the slope of travel time curve ($dt/d\Delta$) has proved to be much more useful in the study of the fine structure of the lower mantle.

A. *Surface wave results and average structure of the upper mantle—a review.* Various local studies have shown the crust and the uppermost mantle to be quite non-uniform. However, at depths greater than about 100 km certain characteristics of the velocity–depth curves seem to be world-wide. These features can be studied

using phase and group velocities of Rayleigh and Love waves in the period range of 50–600 seconds. Measuring these over complete great circle paths provides an accurate method of velocity determination and an objective world-wide average.

The techniques of determining phase and group velocity using the successive passages of Rayleigh and Love waves at a given station have been described in earlier publications (Satô 1958, Toksöz & Anderson 1966). These techniques involve computing the phase delay of each Fourier component of the wave train relative to an earlier passage in the same direction, such as between pairs G_2–G_4 (Love waves), or R_3–R_5 (Rayleigh waves), at the same station. The phase velocity C at a period T is given by:

$$C(T) = \frac{\Delta_0}{\delta t + T[\delta\phi(T) + N - \frac{1}{2}]} \tag{1}$$

where Δ_0 = length of great circle path, $\delta t = t_{n+2} - t_n$ and $\delta\phi(T) = \phi_{n+2}(T) - \phi_n(T)$. t_{n+2} and t_n are initial times of Fourier time windows and ϕ_{n+2} and ϕ_n are phase delays relative to the beginnings of the windows. N is an integer, and the half period phase shift is due to two extra polar passages of one wave train relative to the other.

Surface waves generated by large earthquakes and recorded by long-period seismograph systems at Pasadena and Isabella, in California, and at other stations, have been analyzed for velocity measurements. The great circle paths are shown in Fig. 1. For our present purposes we will discuss only those paths which pass through Pasadena and the regions of Alaska and Mongolia. These paths are, on the average, 60% oceanic and 40% continental, and sample various geologic and physiographic units. The phase and group velocities of Love and Rayleigh waves along these paths are shown in Figs. 2 and 3. These results are tabulated and other details are given by Toksöz & Ben-Menahem (1963) and Toksöz & Anderson (1966).

In order to carry out the interpretation of these dispersion data in terms of a mantle model, a hypothetical 20-km thick crustal model which is a weighted average of oceanic and continental crustal structures was selected. Starting from an initial trial

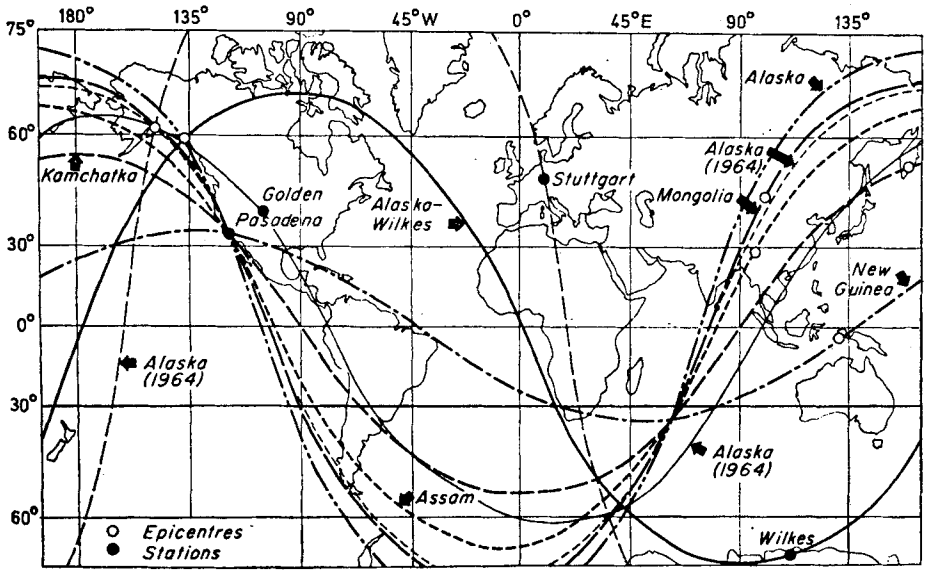

FIG. 1. Great-circle paths from which Love and Rayleigh wave data were utilized.

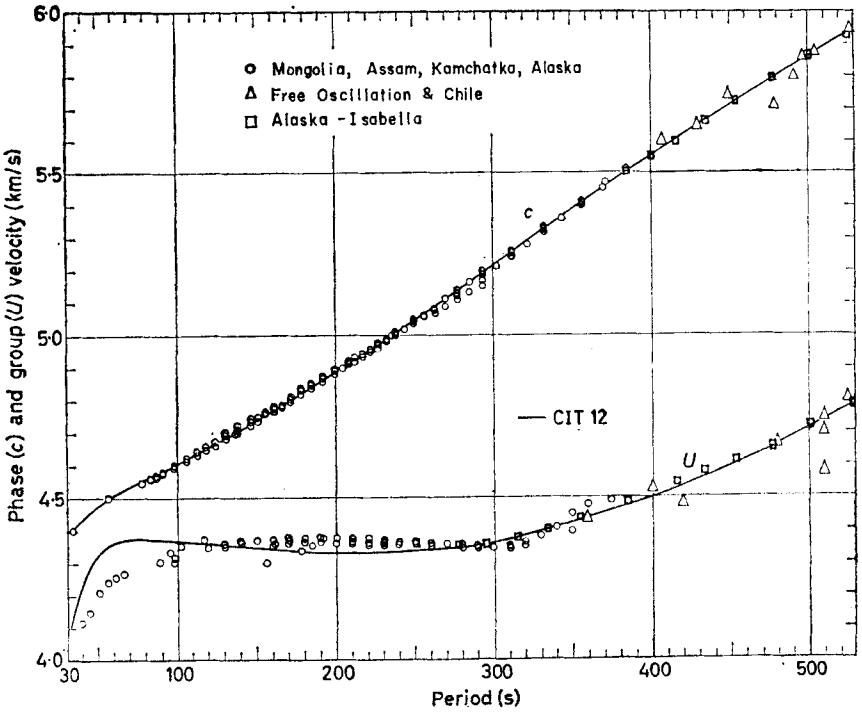

FIG. 2. Love wave dispersion data for a set of close-lying great-circle paths and the theoretical curves of the CIT-12 mantle model.

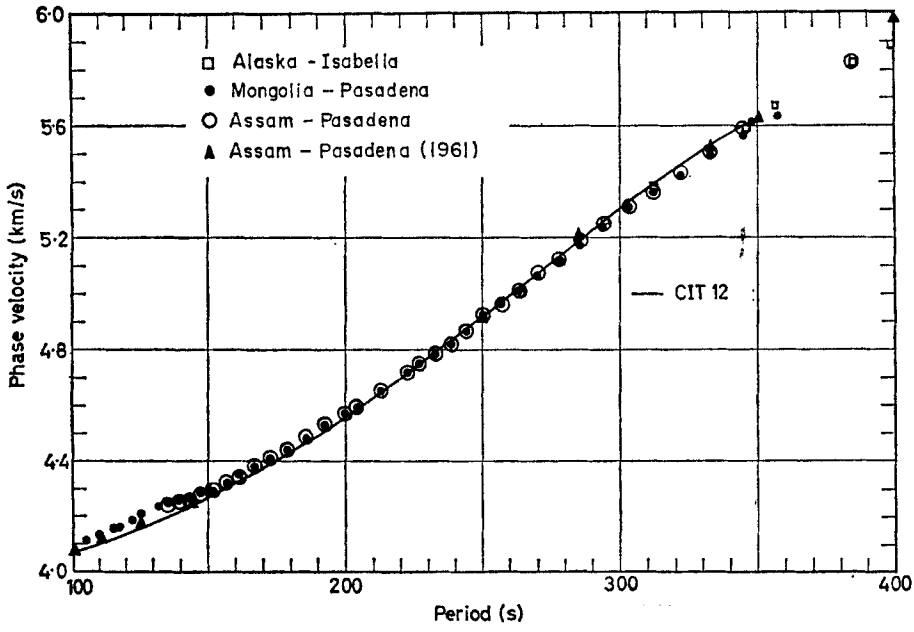

FIG. 3. Rayleigh wave phase velocities for four close paths and the CIT-12 theoretical model.

structure, the mantle model was then modified until good fits to both the Rayleigh and Love wave dispersion data were obtained. The methods used in the computations are described by Alsop (1963), Anderson & Toksöz (1963), and Anderson (1964). In this study only shear velocity was treated as an independent variable in finding the models. The compressional velocities and densities used in the computations were derived from the shear velocities using the values of Poisson's ratio given by Gutenberg (1959), and the velocity–density relationships of Birch (1964). The theoretical dispersion curves of the adopted composite model (CIT-12) fit the data very closely, as shown in Figs. 2 and 3. Fig. 4 shows the smoothed shear velocity profile. Both density and compressional velocity profiles have similar features—a low-velocity zone for compressional waves and a low density region.

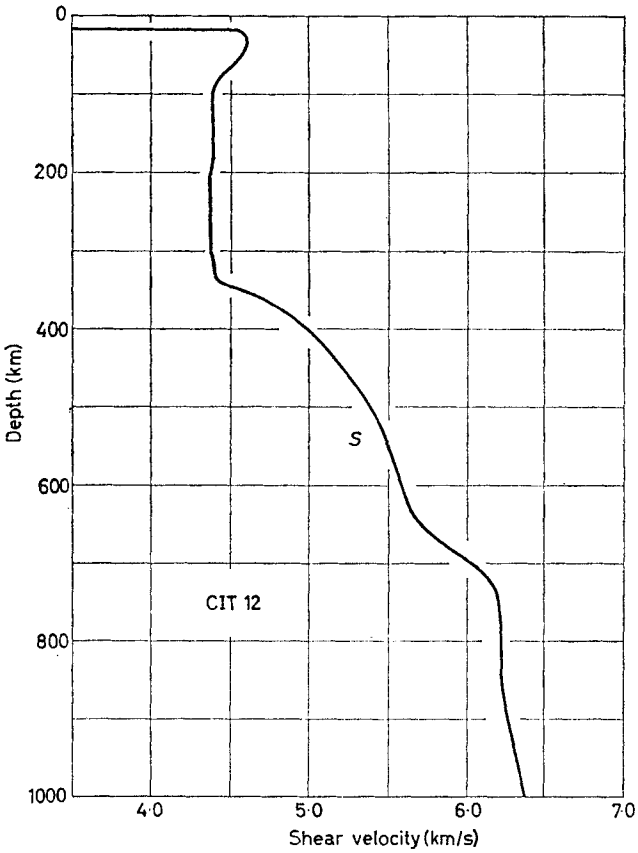

FIG. 4. Shear velocity distribution for the CIT-12 mixed path model.

The major characteristics of the velocity model CIT–12 are: (a) a broad low-velocity zone extending from a depth of 50 to about 350 km, (b) a steep velocity gradient immediately below the low-velocity zone, and (c) another steep gradient at a depth of about 700 km. These two anomalous velocity gradients (centred at depths of 350 and 700 km) are the major inhomogeneities of the upper mantle. They represent regions where the velocity behaviour departs appreciably from that of a homogeneous body.

The seismic body wave evidence for the presence of inhomogeneities in the upper mantle is accumulating with improved observational facilities. From travel time

slopes Niazi & Anderson (1965) determined a compressional wave profile with discontinuities at around 350 and 700 km. *P*-velocity profiles of Archambeau *et al.* (1967), based on travel times from underground nuclear explosions, also contain these discontinuities. Velocity profiles given by Golenetskii & Medvedeva (1965) show similar features. Thus, the evidence for the existence of the discontinuities at depths of about 350 and 700 km is strong for compressional wave vleocities as well as for shear velocities. One feature of the compressional velocity profiles markedly differs from that of the shear profiles: the low velocity zone for compressional waves does not extend to as great a depth. Compressional velocities, in general, start to increase at a depth of about 150 km, in contrast to shear velocities which remain nearly constant to a depth of 350 km.

A detailed investigation of the causes and implications of the low-velocity zone and the discontinuities in the upper mantle are outside the scope of this paper. However, a few remarks may be in order.

The great depth of the zone of relatively low shear velocities is of particular interest. The conventional interpretation is that the upper mantle is a region with a particularly high thermal gradient. The effect of temperature on velocities offsets the effect of pressure. The critical temperature gradient, which gives constant shear velocity with depth, may be defined by:

$$\left(\frac{dT}{dr}\right) = \rho g \frac{(\partial V_s/\partial T)_P}{(\partial V_s/\partial P)_T}, \tag{2}$$

where T = temperature, P = pressure, r = radial distance from the centre of the Earth, ρ = density, g = gravitational attraction. When this gradient is exceeded the velocity will decrease with depth. The critical gradient has been estimated to be between 5 and 8 °C/km (Birch 1952, Clark & Ringwood 1964). If we adopt a value of $T = 600$ °C at 50 km and a gradient of 5 °C/km, the temperature at a depth of 350 km will be about 2100 °C. This value exceeds the extrapolated minimum melting temperature of such materials as 'pyrolite' (Clark & Ringwood 1964). Although possibly not relevant, the critical temperature gradient for MgO is only 2·7 °C/km for shear waves (Schreiber & Anderson 1966). This number is firmer than the above estimates since it is based on precise measurements of the effect of temperature and pressure in the absence of porosity. If the critical gradient is this low then the temperature at 350 km could be as low as 1450 °C and still be consistent with a low-velocity zone to this depth. This is below the estimated melting temperature of mantle material at this depth.

The velocities to 350 km are clearly low, but it is not established that the velocity stays constant or decreases with depth below some 150 km. So it is necessary that the temperature gradient between 150 and 350 km be critical or supercritical. If the higher estimates of critical gradient are shown to be appropriate for ultrabasic rocks and if the velocity gradient between 150 and 350 km requires a thermal gradient of the order of 4° C/km or higher, then partial melting or a changing composition with depth must be invoked to explain the properties of the low velocity zone below 150 km. On the basis of available seismic data it is not clear that partial melting is required, but neither can it be ruled out. This is an important problem that requires more detailed seismic information as well as high temperature and high pressure studies to establish the melting behaviour and the temperature and pressure derivatives of velocity of mantle material.

The difference between the shear velocity profile given in Fig. 4 and the compressional velocity profiles referenced earlier (that is, the *P*-wave velocity increasing with depth while the *S*-velocity remains relatively constant in the depth range of 150–350 km) can also be explained in terms of temperature effects on velocities. There is evidence that the effect of pressure on *P*-wave velocity is relatively greater than on shear velocity, while the temperature effect is greater on *S*-wave velocity (see Clark &

Ringwood 1964, for detailed discussion). Then, it is not unreasonable to expect an increase in *P*-wave velocity with depth while the *S*-velocity remains constant or decreases.

The nature and causes of discontinuities in the upper mantle have been the subject of many discussions in terms of possible phase changes (Ringwood 1962, Birch 1964). A review of these may be found in Clark & Ringwood (1964) and Anderson (1967). Because of our lack of knowledge of the mineralogical constitution of the upper mantle, it is hard to say which, if any, of these proposed phase changes is most likely. In addition, changes in chemical composition at these discontinuities cannot be ruled out.

B. *'Discontinuities' in the lower mantle.* The determination of the fine structure of the seismic velocity profile is more difficult in the lower mantle than it is in the upper mantle. The fundamental modes of surface waves and free oscillations that are affected by the lower mantle are of very long periods and lack resolving power necessary for determining the finer features of the velocity variations. Furthermore, at long periods, density becomes a significant variable, and the effects of variations in density and velocity cannot be determined separately from dispersion data (Anderson 1964, Takeuchi *et al.* 1964, Landisman *et al.* 1965). Travel times of body waves, especially those measured using earthquake data, require considerable smoothing before they can be used for structural interpretations. This is partly because of uncertainties in location of the source, and partly because of the effects of structure under the stations and the source area. These station and source corrections added to the measurement accuracies often exceed the effects of velocity inhomogeneities. Current mantle models represent smoothed averages of the actual conditions at depth.

The seismic waves from nuclear explosions have yielded more accurate travel time data because of exact knowledge of the source parameters and improved observational facilities. These new travel times show certain departures from the travel time tables of Jeffreys & Bullen (1958) in the distance range of $\Delta = 30°$ to $100°$. Most of these are listed in the literature as J–B residuals, a quantity which is the difference between the J–B travel time and the observed value at a given distance (Doyle & Webb 1963, Carder 1964, Cleary & Hales 1966, Herrin 1966, Carder *et al.* 1966).

With the establishment of seismic arrays, such as LASA (Large Aperture Seismic Array) in Montana and the extended array at TFSO (Tonto Forest Seismic Observatory), a new approach to the problem of determining seismic velocity with depth has become feasible. It is now possible to measure the slope of the travel time curve ($dt/d\Delta$) directly, and, using the $dt/d\Delta$ vs Δ data and the Weichert–Herglotz formula, the velocity variation with depth can be determined in a more accurate and direct fashion than is possible with travel times alone. In this section we will briefly describe such a study. Using the $dt/d\Delta$ data computed from arrivals at LASA for events at distances of more than $\Delta = 30°$ together with the travel times from the Long Shot explosion, a velocity–depth curve which suggests the presence of 'discontinuities' in the lower mantle can be determined. A much more detailed discussion is given in a separate paper by Chinnery & Toksöz (1966).

The Large Aperture Seismic Array (LASA) consists of twenty-one subarrays. The geometry of the subarrays is shown in Fig. 5 and details of instrumentation, etc., can be found in Green *et al.* (1965). The measurement of $dt/d\Delta$ was made from the set of delay times observed at the eight outer subarrays for each event. A plane was fitted to the wave front by a least squares procedure and an apparent azimuth and travel time slope was calculated. The epicentral distance and focal depth information for each event were obtained from the USCGS PDE cards. The epicentral distance was corrected for focal depth by projecting the ray path back to the Earth's surface, using the observed value of $dt/d\Delta$, and a simple velocity structure. The station-epicentre azimuth was computed using the epicentre co-ordinates and this was compared with the measured azimuth as a check on the reliability of the $dt/d\Delta$ measurement.

Most of the events recorded at LASA arrive from two narrow ranges of azimuth These are 300–320° and 140–160°, measured clockwise from the north at LASA. The first includes Alaska, the Aleutian Islands, the Kurile Islands, and Japan, and only events from this direction were chosen for structure study. This was done to eliminate systematic differences in measured $dt/d\Delta$ due to path differences. These differences will be discussed in greater detail in the next section. Another reason for the choice of 300–320° events was the Long Shot explosion of 1965 October in Amchitka Island. Travel times as well as amplitudes from the North American recordings of this shot were used as additional data, both for interpretation and static correction of the measured $dt/d\Delta$ values. Fig. 6 shows the azimuth range 300–320°, and the location of Long Shot.

Travel time slopes were measured from 167 events in the distance range of 25–92° and these are displayed as a function of distance in Fig. 7. $dt/d\Delta$ computed from the Jeffreys–Bullen tables are also shown in the figure. In spite of scatter, the mean of the observations deviate from the J–B curve by an amount greater than the average scatter. This is especially clear at about $\Delta = 45°$, 62° and 90°. The nature of these deviations is such that they oscillate around the J–B curve, and this immediately suggests that the velocity–depth curve must also deviate from the Jeffreys model.

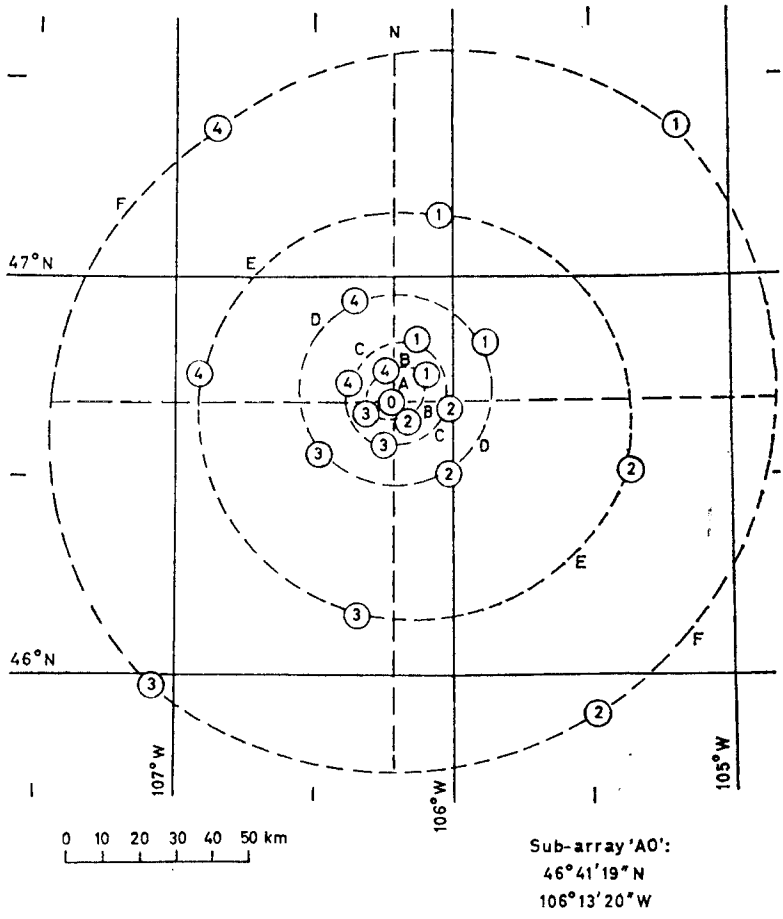

FIG. 5. The Large Aperture Seismic Array (LASA) showing the locations of the twenty-one sub-arrays.

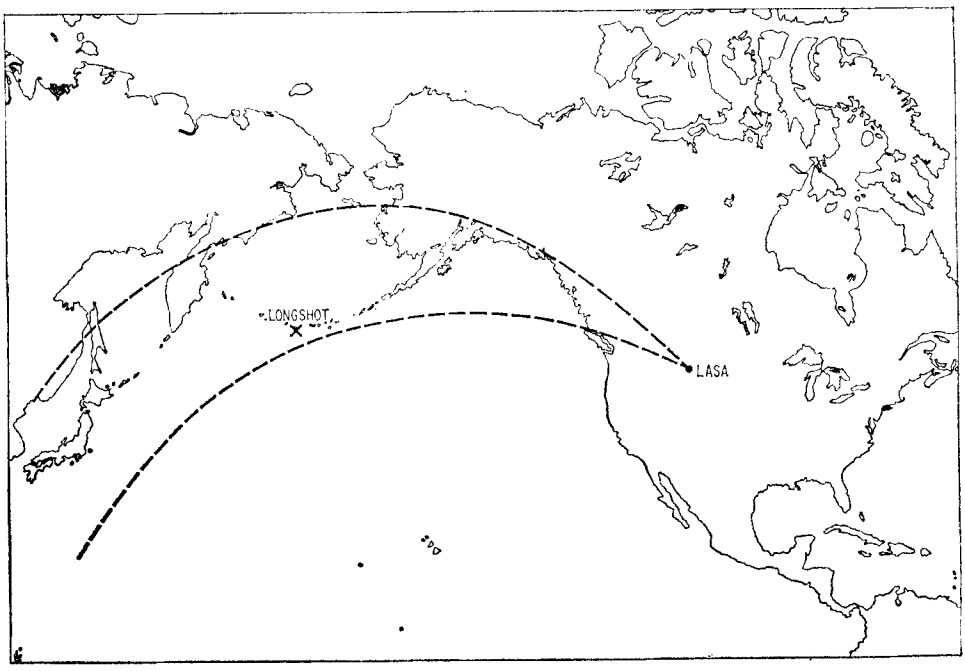

FIG. 6. Locations of the LASA and the Long Shot nuclear explosion. The dashed lines outline the azimuth range 300°–320° from LASA.

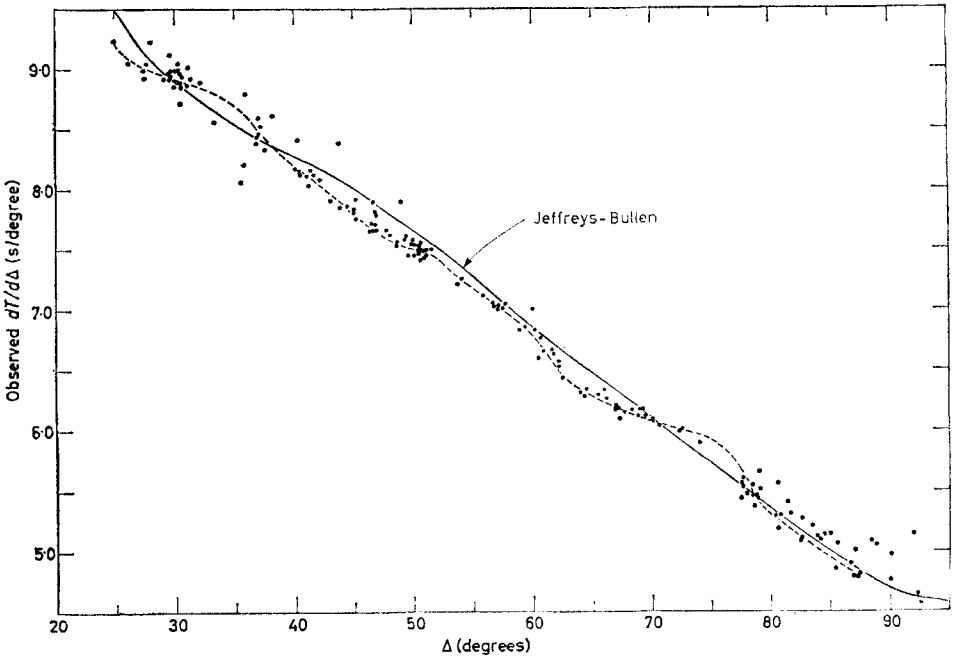

FIG. 7. Observed $dt/d\Delta$ for all events in the azimuth range 300–320° detected at LASA. The dashed curve is the adopted ' mean ' curve.

The reasons for the scatter in the data are timing errors, inaccuracies in epicentral location and focal depth, azimuthal variations within the range concerned, and the effects of local geology at LASA. A set of criteria was established empirically to separate out the most consistent events. These requirements included that the ground amplitude at LASA be greater than 25 millimicrons, and that the measured azimuth at LASA deviate by less than 1·5° from the computed azimuth. Although these conditions reduced the number of usable events by 50% they also reduced the scatter to less than ±0·05 seconds per degree, and did not change the shape of the major characteristics of the $dt/d\Delta$ vs Δ curve.

The absolute travel time t_0 at a distance Δ_0 is given by:

$$t_0 = \int_0^{\Delta_0} dt/d\Delta \; d\Delta. \tag{3}$$

Graphically, this is the area under the $dt/d\Delta$ vs Δ curve and it gives us a means of computing the travel time from the slopes measured using LASA. The travel times from earthquakes are limited in accuracy mainly because of uncertainties in the epicentre and origin time. These affect the slopes less seriously. Explosions, on the other hand, being free of source uncertainties, provide very accurate travel-time data. The differences between J–B tables and observed travel-times ($R \equiv t - JB$) from Long Shot, Bilby (fired on 1963 September 13 at Nevada Test Site) and explosions in the central Pacific are shown in Figs. 8, 9, and 10 respectively. These residuals are related to the travel time slopes by

$$R(\Delta_0) = \int_0^{\Delta_0} [(dt/d\Delta)_{\text{observed}} - (dt/d\Delta)_{JB}] d\Delta. \tag{4}$$

The curves in Figs. 8, 9, and 10 are the curves computed using (4) and Fig. 7, and are shifted along the ordinate to account for travel time differences in the crust and upper mantle under the shot point. From the fit of the travel time residuals obtained by the

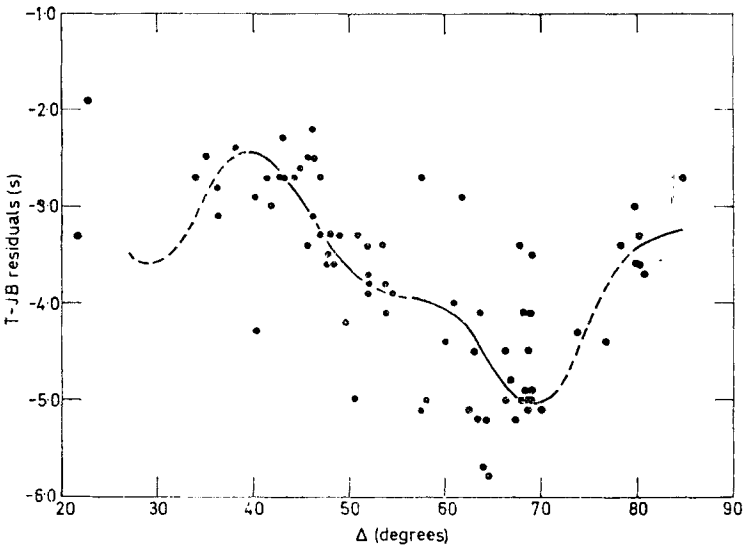

FIG. 8. Travel-time residuals (*T–JB*) observed at stations in North America and Europe from the Long Shot explosion after applications of station corrections. The curve is predicted residuals from dashed line in Fig. 7 after a +0·05 seconds/degree correction.

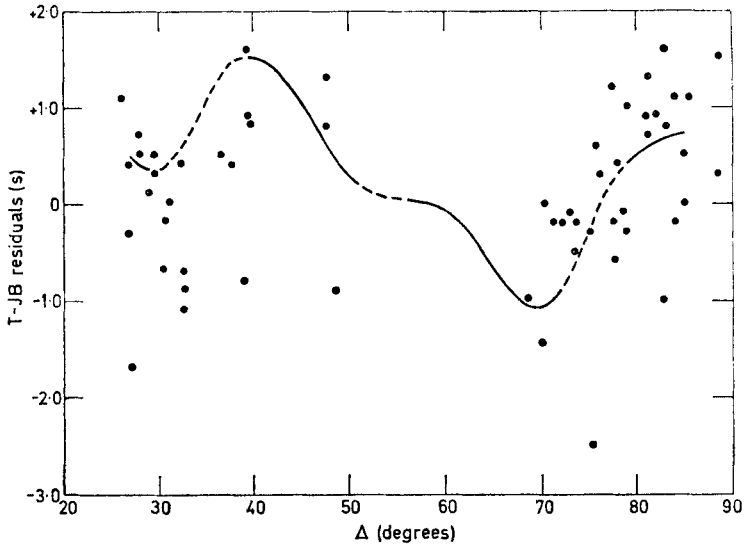

FIG. 9. *T–JB* residuals from Bilby explosion observed at fifty-eight stations in North America and Europe after application of station correction. The curve is the same as that in Fig. 8 except for vertical adjustment (source correction).

two methods, it is clear that the features of the $dt/d\Delta$ curve are indeed due to conditions in the mantle and not to local effects at LASA. The station corrections at the array have a considerable magnitude, and they vary with the azimuth of the wave path to the array. For a given azimuth and teleseismic distances, however, the corrections should be very nearly constant for all events. To match the travel times from Long Shot to the values obtained by integrating the $dt/d\Delta$ curve, a static correction of +0·05 s/deg was applied (see Chinnery & Toksöz (1966) for extended discussion) to the $dt/d\Delta$ vs. Δ curve.

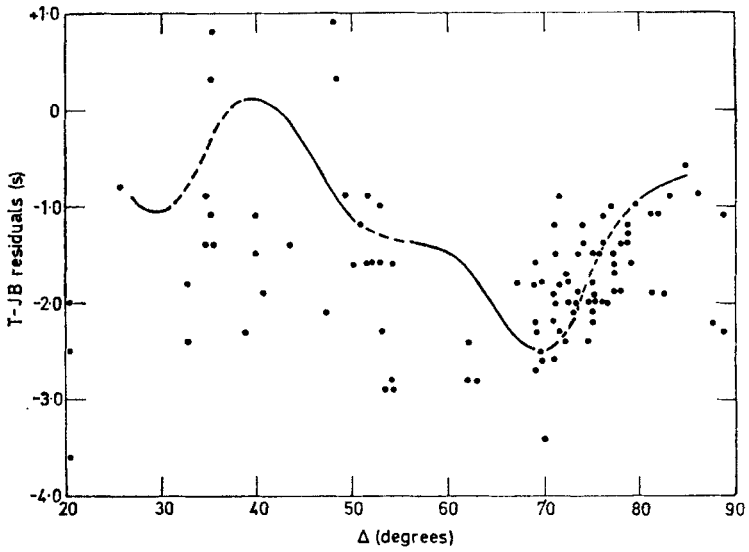

FIG. 10. *T–JB* residuals from nuclear explosions in the Central Pacific. Station corrections are applied where available. The continuous curve is the same as that in Fig. 8 except for the vertical adjustment.

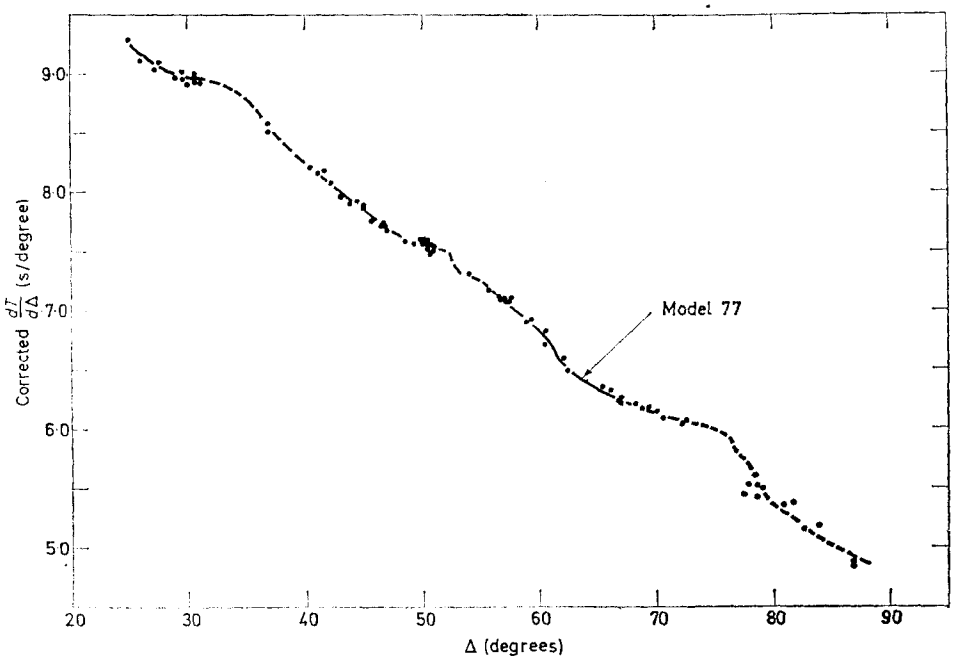

FIG. 11. The comparison of the observed $dt/d\Delta$ (' good ' events from Fig. 7) and the theoretical values from Model 77.

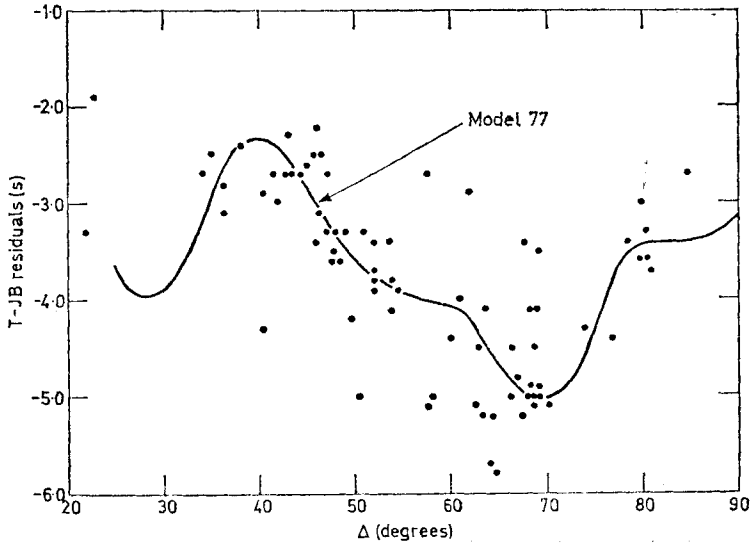

FIG. 12. The comparison of the observed travel times from Long Shot (Fig. 8) and the theoretical times from Model 77.

The determination of the velocity structure of the mantle from the inversion of $dt/d\Delta$ vs Δ and the travel time residuals was carried out by a trial and error method. Starting from the Jeffreys–Bullen velocity model, successive perturbations were made until a good fit to the $dt/d\Delta$ curve was obtained. Because of the lack of information at close distances, direct inversion by means of the Weichert–Herglotz formula was not attempted. For the same reason, the upper mantle structure could not be determined directly. A model was chosen based on crustal information, surface wave data (see previous section) and regional upper mantle studies down to a depth of 600 km. The only direct constraints on this hypothetical model were the known crustal structure and the travel-time residuals at distances of 25–30°. To fit these residuals, the upper mantle velocities were increased beyond those of other models.

The effect of upper mantle structure on the $dt/d\Delta$ values beyond $\Delta = 30°$ is very small. The $dt/d\Delta$ values are extremely sensitive to the velocity gradient at the lowest point of ray path. Thus, the use of a hypothetical model to a depth of 600 km, does not affect the reliability of the velocity structure below this depth.

Our velocity model based on LASA data and the Long Shot travel times is designated as Model 77. The agreement between the theoretical and observed values of $dt/d\Delta$ and the corresponding J–B residuals are shown in Figs. 11 and 12. In both cases the fit can be termed as being very good.

An additional piece of information that can be utilized in testing the reliability of the model is the variation of the amplitude of *P*-wave arrivals with distance. If we neglect the effects of attenuation and geometric spreading, which are smooth functions. the amplitude variation with distance is a function of the change of velocity gradient with depth (Asbel *et al.* 1966). This can also be expressed in terms of $d^2T/d\Delta^2$ (Bullen 1963). Unfortunately, it is very difficult to obtain reliable amplitude data. The difficulties stem from the effects of (a) the ground under the station (i.e., where

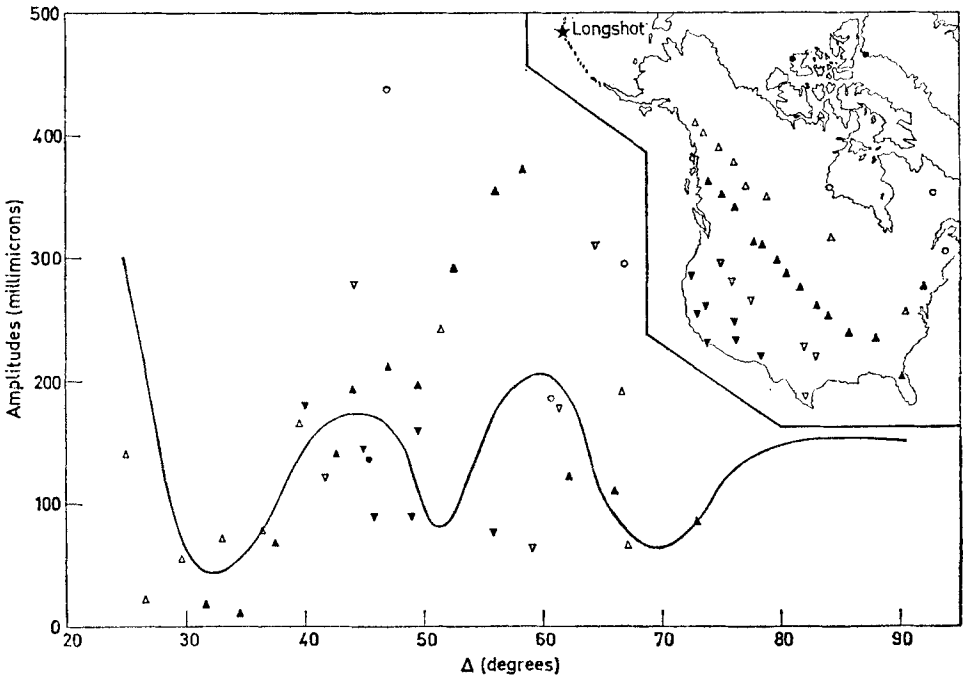

FIG. 13. Observed amplitudes of *P*-waves from the Long Shot recorded at LRSM stations in North America. Insert map shows the locations of the stations. Continuous curve is the theoretical $d^2t/d\Delta^2$ (amplitude factor) from Model 77.

velocities are low, amplitudes are large), (b) the radiation pattern at the source (most earthquakes and some explosions have non-uniform radiation patterns), and (c) uncertainties in instrumental magnifications and ground-coupling coefficients. Using only Long Shot data recorded at well-calibrated LRSM stations in North America, we compared the observed amplitudes with the variation of $d^2t/d\Delta^2$ predicted from Model 77. This is given in Fig. 13. The agreement is good to about $\Delta = 46°$, and beyond this the scatter in the observed data is too large for the comparison to be conclusive.

The variation of seismic compressional wave velocity in the mantle (Model 77) is shown in Fig. 14 and tabulated in Table 1. We should repeat here that the upper portion of the model down to a depth of 600 km (shown in Fig. 15) is hypothetical and based on other studies. Below this depth, however, the model is reliable except at depths corresponding to regions where there are gaps in observed $dt/d\Delta$ data, such as at $\Delta = 34°, 38°, 53°$, and $75°$. Within these regions the velocity structure appears to be anomalous, and they are discerned further below. The absolute accuracy of the velocity distribution is difficult to estimate and is determined by the accuracy of the data. Since the $dt/d\Delta$ observations were the most accurate, velocity gradients given by Model 77 must be very reliable. The good agreement with the travel-time residuals is evidence for the reliability of the absolute values of the velocity in the lower mantle.

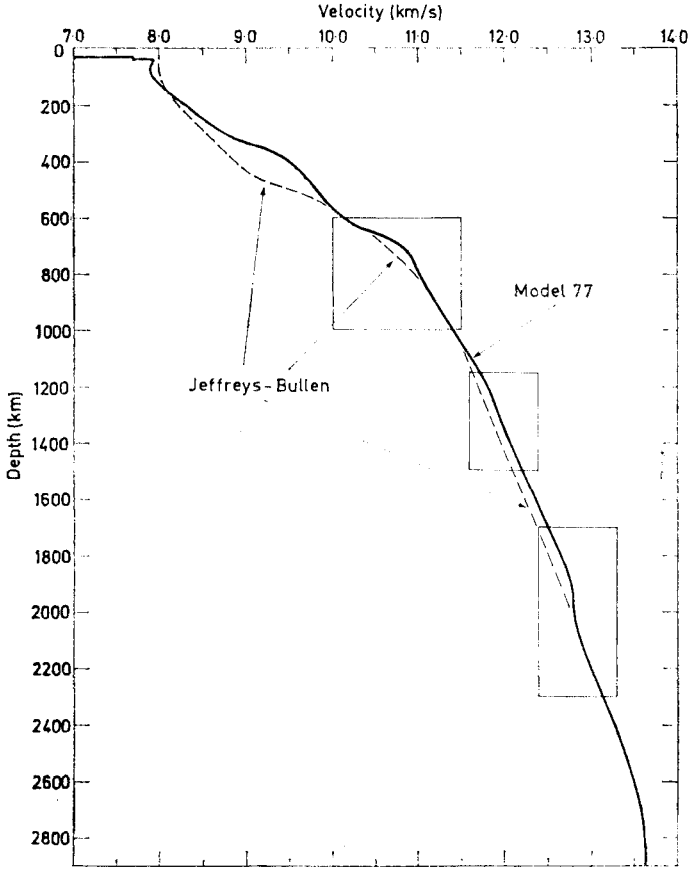

FIG. 14. Compressional velocity profile of the Mantle Model 77, with the Jeffreys–Bullen model for comparison. Boxes show the regions of the ' discontinuities '.

Table 1

The Model 77 velocity distribution in the mantle with the Jeffreys–Bullen model for comparison.

(Parentheses indicate uncertainty because of insufficient data)

Depth (km)	Velocity (km/s) JB	Model 77	Depth (km)	Velocity (km/s) JB	Model 77
40	7·75	(7·80)	1450		12·13
50		(7·95)	1500		12·20
100	7·95	(7·90)	1550		12·27
150		(8·09)	1600	12·26	12·34
200	8·26	(8·28)	1650		12·42
250		(8·47)	1700		12·51
300	8·58	(8·69)	1750		12·59
350		(9·21)	1800	12·53	12·66
400	8·93	(9·44)	1850		12·72
450		(9·63)	1900		12·76
500	9·66	(9·80)	1925		12·78
550		(9·94)	1950		(12·79)
600	10·24	(10·12)	1975		(12·80)
650		(10·44)	2000	12·79	(12·81)
700	10·67	10·76	2025		(12·82)
725		10·86	2050		(12·84)
750		10·93	2100		12·89
775		10·96	2150		12·94
800	11·01	(11·00)	2200	13·03	13·00
850		(11·09)	2250		13·07
900	11·25	(11·20)	2300		13·14
950		(11·31)	2350		13·21
1000	11·43	11·42	2400	13·27	13·27
1050		11·52	2450		13·33
1100		11·62	2500		13·39
1150		11·71	2550		13·44
1200	11·71	11·80	2600	13·50	(13·49)
1225		11·84	2650		(13·53)
1250		11·87	2700		(13·57)
1275		(11·89)	2750		(13·61)
1300		(11·92)	2800	13·64	(13·63)
1325		(11·96)	2850		(13·64)
1350		(12·00)	2900	13·64	(13·64)
1400	11·99	12·06			

The amplitude data support the changes of velocity gradients and the existence of the 'discontinuities'.

The 'discontinuities' in the lower mantle are the most significant features of the model. These are located at depths of about 700, 1200, and 1900 km, and they produce measurable effects on $dt/d\Delta$ curve at distances of $\Delta = 35°$, 52°, and 70°. The exact nature of the behaviour of the velocity curve at the anomalous regions cannot be determined at this stage. It is not clear whether the dV/dr curve changes continuously or discontinuously. Neither is it clear whether the velocity gradient always remains positive or if the velocity actually decreases at these discontinuities. Considering the great depths and the associated high pressures, it is questionable whether an actual velocity decrease (or low velocity regions) would exist in the lower mantle. The mantle–core boundary, where composition might change, could be a possible exception.

This study presents probably the best evidence of the existence of discontinuities in the lower mantle through the interpretation of travel times, directly measured slopes ($dt/d\Delta$) and the amplitudes ($d^2t/d\Delta^2$). There have been less direct indications of lower mantle discontinuities. Gutenberg (1958) suggested regions at depths of

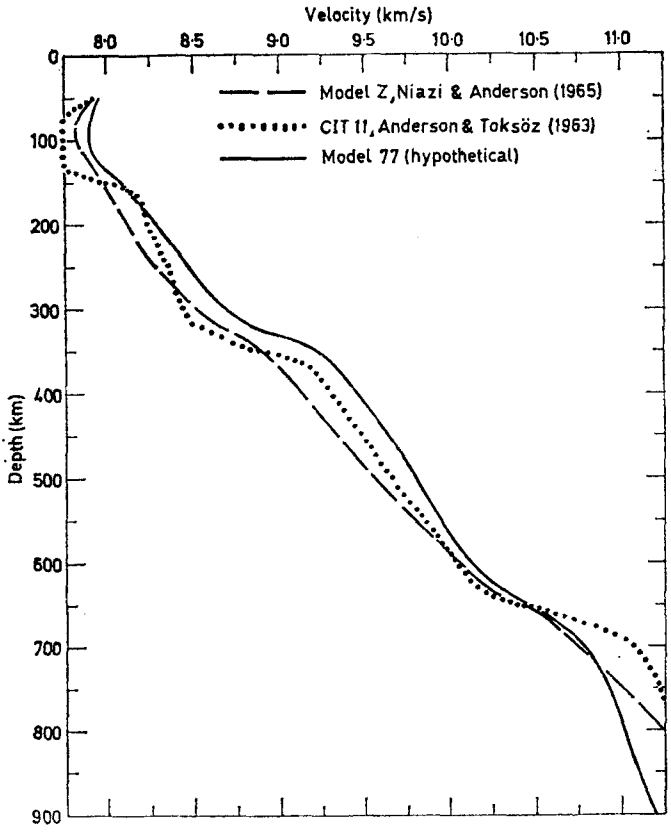

FIG. 15. Upper mantle compressional velocity profiles. Model 77 is hypothetical, and it satisfies the travel time and $dt/d\Delta$ observations at $\Delta=27°$.

h = 900–1000 km and h = 1400–1500 km from amplitude studies as being anomalous. Bugayevskii (1964) has presented evidence of discontinuities in the travel time curve at distances of 36–37°, 51–53°, and 70–73°. These are in agreement with our results, and may suggest the world-wide presence of these discontinuities. The similar features of travel-time residual curves based on data from explosions at widely separated regions (Figs. 8, 9, 10) also point to the universal nature of discontinuities. Another characteristic of these anomalous regions of the mantle may be implied from results of Vvedenskaya & Balakina (1959). They measured P and SH wave amplitude ratios and detected anomalies at Δ = 38–42°, 51–53°, and 70°. These results imply different behaviour for P and S wave velocity profiles at depths corresponding to the anomalies. A direct study of S-wave travel times and slopes is now under way for further investigation of the differences between P and S wave profiles.

In a similar study using TFSO records and events from all azimuths, Johnson (1966) found second-order discontinuities at depths 840 and 1150 km and less pronounced ones at 1300, 1700, and 1950 km.

In summary, we may state that there are discontinuities in the mantle at depths of about 350, 700, 1200 and 1900 km where seismic velocity gradients exhibit anomalous behaviour. Although details of the anomalies may vary from one region to another, the evidence points to the universal nature of these discontinuities and the inhomogeneity of the lower mantle.

3. Lateral inhomogeneities in the mantle

Variations in crustal structure as well as differences in the sub-Moho (P_n) velocities over different regions of the Earth have been well established by refraction studies (Kosminskaya & Riznichenko 1964, Pakiser & Steinhart 1964, McConnel *et al.* 1966). Measured P_n velocities, for example, vary between 7·7 and 8·5 km/s, with the lower values being associated with active tectonic areas. Regional surface wave data (Alexander 1963, Brune & Dorman 1963, Dewart & Toksöz 1965) also show that regional variations in shear velocity profiles are quite pronounced and continue into the low velocity zone. The question that remains, however, is the depth to which these lateral inhomogeneities extend.

In this section we will look at the seismic surface wave and body wave data as well as gravity results for the study of inhomogeneities.

A. *Regional structure of the upper mantle.* The phase velocities of mantle Love and Rayleigh waves have been measured over great-circle paths in the period range between 80 and 666 seconds (Toksöz & Ben-Menahem 1963, Toksöz & Anderson 1966). The distribution of great-circle paths (Fig. 1) shows that most regions of the world have been sampled. Love wave data exist for all paths, while Rayleigh wave data exist only for those paths discussed in the previous section. For this reason, only Love waves were used in the present study.

Comparison of velocities over different great-circle paths shows that where the paths are close, the velocities are in good agreement (better than 0·5%). Where paths traverse different regions, however, the differences in phase velocities are significant, and these are more pronounced at relatively short periods.

Interpretation of these composite phase velocity data in terms of mantle structure is a complex problem. The paths are not sufficiently dense for a comprehensive analysis such as dividing the Earth's surface into a mesh of homogeneous units, each of which is, say, 5° × 5°. Thus, we must follow a less objective procedure. As a first step, we

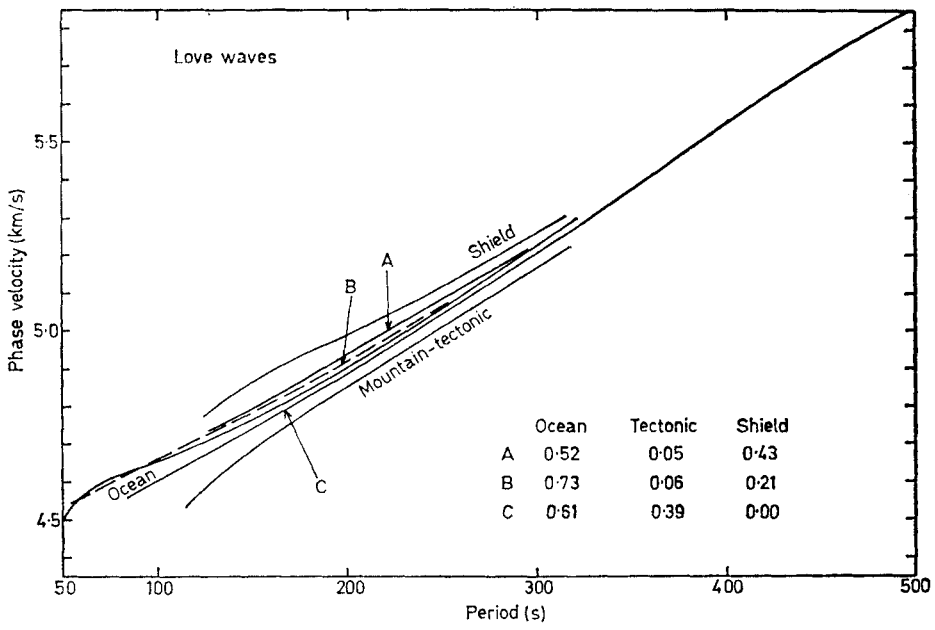

FIG. 16. Observed composite path Love wave data and the extracted ' pure-path ' phase velocities.

attempted to correlate the phase velocities of the composite paths with the relative fractions of the oceanic and continental regions traversed. This correlation was poor. Velocities varied over paths which had equal fractions of oceanic segments, and velocities were higher over paths which traversed more continental shield areas. As a second step, we (Toksöz & Anderson 1966) divided the Earth into three regions: ocean, continental shield, and tectonic. These were determined on the physiographic features alone. Continental margins were taken as continents; active zones and highly mountainous areas were considered tectonic. Effects of ocean ridges were neglected. With this division it was assumed that the overall phase delay of a surface wave on a given great-circle path was a linear function of the individual phase delays over various segments (ocean, shield, tectonic). It was further assumed that the phase shifts due to boundaries of regions and deviations from great-circle paths were negligible.

With these assumptions, and knowing the percentages of paths through each region, pure-path phase velocities were computed. Observed Love wave data and computed pure-path velocities are shown in Fig. 16. This shows that shield areas are characterized by the highest phase velocities, while the tectonic regions have the lowest velocities. The differences are greater at shorter periods as one might expect. Because of the limited number of paths with long period data, no separation could be made at periods longer than 320 seconds.

The determination of velocity structures in the upper mantle under the oceanic, shield and tectonic areas was carried out using the pure-path phase velocities with the

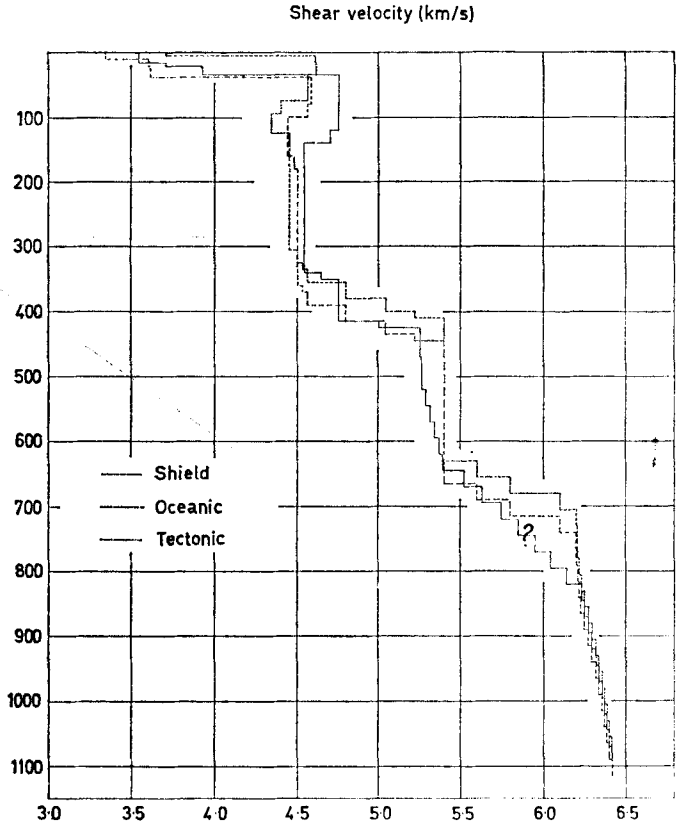

FIG. 17. Upper mantle shear velocity models for the oceanic, continental shield, and tectonic regions. Below 500 km profiles are uncertain because of insufficient data.

same procedure discussed in Section 2. For each area, the crustal structure was chosen as the average of those determined by the regional studies. Densities were assumed to vary linearly with shear velocity for each model. The computed shear velocity models are shown in Fig. 17. In addition to differences in the crustal structures, there are significant differences in the structures of the low velocity zones. Below a depth of 500 km, it is not clear whether systematic differences between the oceanic and shield structures persist. This uncertainty arises because the amount of dispersion data at periods longer than about 320 s is too limited to permit the extensions of 'pure-path' phase velocity curves to longer periods. We assumed that all curves must join at about 500 s. This, of course, forced the shield structure to have lower velocities below a depth of about 500 km. There is no evidence to indicate that the Earth's mantle must be laterally homogeneous below a certain depth. In fact, the body wave travel times and travel-time slopes indicate that there are variations in the mantle structure both at shallow and at great depths.

The variations of compressional velocity profiles in the upper mantle are best indicated by the travel-time residuals at stations located on shield or tectonic regions. These differences could be as large as 4 s (Herrin 1966, Toksöz & Folinsbee 1966), and are much too large to be explained in terms of crustal structures alone. Thus, there must be some differences in the upper mantle compressional velocity structures

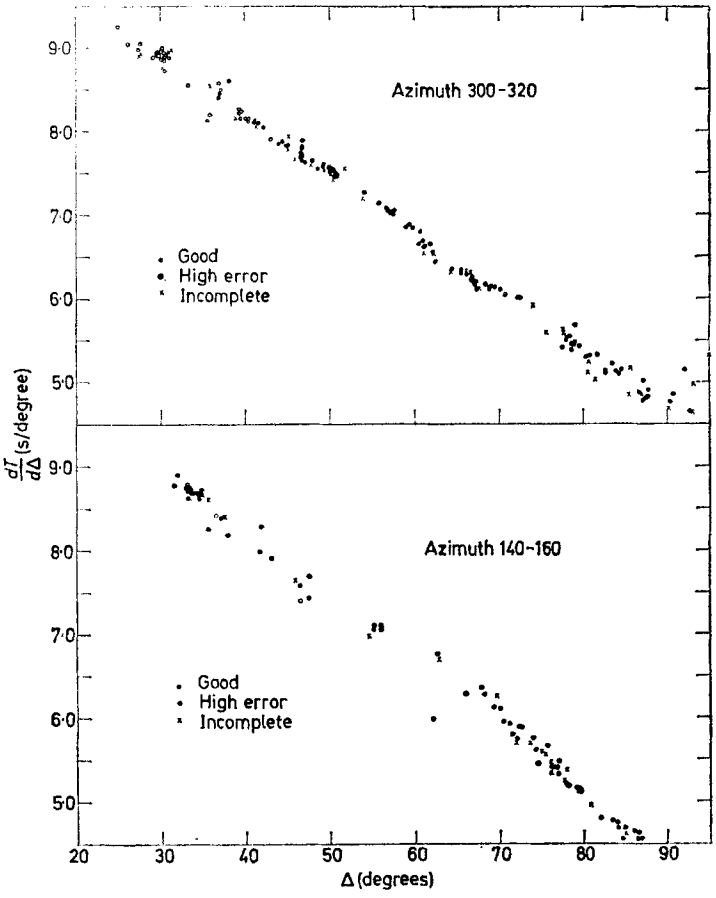

FIG. 18. Observed $dt/d\Delta$ for all events from the azimuth ranges 300–320° and 140–160° from the LASA. These demonstrate the differences between the two different paths.

similar to the shear wave velocities shown in Fig. 17. Another example of this can be found in comparing the JB residuals shown in Figs. 8, 9, and 10. The difference between the average values indicates the differences in transit time in the crust and upper mantle of the source region.

B. *Lateral inhomogeneities in the lower mantle.* The presence of lateral inhomogeneities in the lower mantle is suggested by recent $dt/d\Delta$ measurements with LASA. Fig. 18 shows the variation of $dt/d\Delta$ with Δ, observed from events lying within two narrow ranges of azimuth. The upper curve shows the data from the azimuth range 300–320° (Alaska–Aleutians–Kuriles–Japan regions), and the lower curve corresponds to events from 140–160° (Mexico–Central America–Peru–Chile regions). In these graphs, the events indicated by a cross were timed at only seven of the eight outer subarrays of LASA (due to excessive noise or instrumental failure), and are somewhat less reliable than the other data. Events shown by an open circle give high standard deviation when a plane was fitted to the wavefront by a least squares procedure. Thus, in most instances, this indicates a strong curvature to the wavefront. As we mentioned previously, each curve may be moved a small amount parallel to the ordinate axis to take account of local structure at the array.

Events along the southerly azimuth are clearly very sparse within the distance range 35–65°. However, the coverage is good from 65–87°, and at these distances the two curves differ considerably, particularly in slope. The average slope of the upper curve is approximately 0·65 (seconds per degree per degree), and for the lower curve is approximately 0·93. This difference in slope cannot be explained by the scatter of the data points. It is also unlikely to be due to local effects at LASA since within this distance range the angles of incidence change at most by 6°. We are forced to conclude, therefore, that we have an indication of significant differences in velocity gradient at depths of 1800–2600 km in the mantle.

The general incompleteness of the data, particularly along the southerly azimuth, does not permit a more detailed investigation of these differences at the present time. It will be interesting to see if further data from LASA and other arrays substantiate the interpretation presented here.

C. *Temperature variations under oceans and continents.* Temperature is likely to have a strong effect on the behaviour of materials in the mantle, particularly in the upper mantle. Below an accessible depth of a few kilometres, the thermal state of the Earth must be determined indirectly using geophysical and geochemical data. There have been many observations of heat flow at the surface of the Earth. However, the other data needed for the determination of temperature at depth (i.e. the distribution and abundance of heat sources, mode of heat transport, thermal conductivity, opacity of mantle materials, and thermal history) are not known well enough for an accurate calculation. Indirect analyses based on different models yield temperature profiles that differ significantly (Lubimova 1958, MacDonald 1959, 1961). The observed heat flow data show no great systematic variations between oceanic and shield type continental regions (Lee 1963). This, together with the differences in composition and radioactivity concentration in oceanic and continental crustal rocks, leads to the conclusion that temperatures must vary in the upper mantle under different regions. MacDonald (1963) and Clark & Ringwood (1964) computed temperature profiles which varied under oceans and continents, the oceanic mantle having the higher temperature at a given depth.

In the upper mantle, seismic velocities are very strongly affected by temperature and pressure. At any given depth the pressure effects are roughly the same for all areas. The bulk composition of the mineral assemblages that are likely to constitute the upper mantle in the various regions does not differ greatly in its seismic velocities at a given pressure and temperature. The variation of seismic velocity profiles under

oceanic and continental regions, such as those shown in Fig. 17, can be used to estimate the maximum temperature differences between these regions.

The temperature difference we compute will be a maximum under the assumption that continents were derived from the underlying mantle. The net effect is to raise the velocity and density of the mantle since the less dense, lower velocity material is removed to form the continent. This process also tends to remove heat and radioactivity from the upper mantle and to raise the effective melting point. The effective temperature and the overall elastic properties would both tend to be less under continents than under oceans, assuming conditions were initially identical. By ignoring the possible effect of differences in composition we will get an upper limit on the difference in temperature between oceans and continents if the continental mantle is, indeed, depleted of low velocity–low density material.

We can express the velocity (V) variation with depth (z) in a homogeneous region as

$$\frac{dV}{dz} = \left(\frac{\partial V}{\partial P}\right)_T \frac{dP}{dz} + \left(\frac{\partial V}{\partial T}\right)_P \frac{dT}{dz}. \tag{5}$$

Now, let us compare continental shield areas with oceanic basins. Velocities under these regions are denoted by subscripts 'c' and 'o', respectively. Writing (5) for shields and oceans, and subtracting, we obtain

$$\frac{dV_c}{dz} - \frac{dV_o}{dz} = \left[\left(\frac{\partial V_c}{dP}\right)_T - \left(\frac{\partial V_o}{\partial P}\right)_T\right] \frac{dP}{dz} + \left(\frac{\partial V_c}{\partial T}\right)_P \frac{dT_c}{dz} - \left(\frac{\partial V_o}{\partial T}\right)_P \frac{dT_o}{dz}. \tag{6}$$

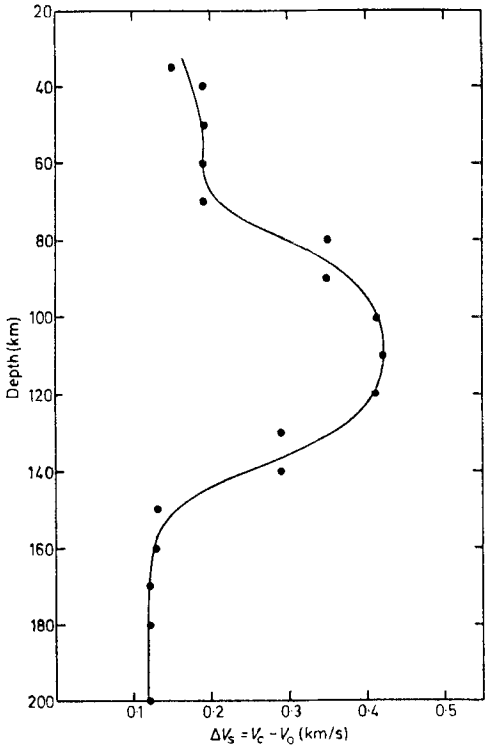

FIG. 19. Difference between the shear velocities of the oceans and the continental shield models shown in Fig. 17. The curve is smoothed to remove effects of steps.

Equation (6) can be simplified by including some approximations. Firstly, the pressure effect on oceanic and shield regions should be nearly the same. Thus, the first term can be neglected. Secondly, the temperature coefficient of velocity in the mantle can be assumed to be the same under both oceans and continents, in the absence of data indicating otherwise. With these assumptions, we can write

$$\frac{d}{dz}(V_c - V_o) \doteqdot -\left[\frac{d}{dz}(T_o - T_c)\right]\left(\frac{\partial V}{\partial T}\right)_P. \tag{7}$$

If $(\partial V/\partial T)$ is a constant with depth, the relationship between the temperature difference $\Delta T = T_o - T_c$ and velocity variation $\Delta V = V_o - V_c$ can be written as:

$$\Delta T(z) = -\Delta V(z)\Big/\left(\frac{\partial V}{\partial T}\right) + C, \tag{8}$$

where C is a constant. ΔV can be evaluated at each depth from shear velocity models of Fig. 17, and it is shown in Fig. 19. $\partial V/\partial T$ must be determined experimentally for chosen petrologic models.

There are a limited number of laboratory measurements of temperature coefficients of shear velocity at elevated temperatures and pressures. The data of Hughes & Maurette (1957) for basic igneous rocks cover a very limited range up to 6 kb and 400 °C. The measurements of Susse (1961) for MgO extend to 1200 °C, and values averaged according to Voigt's scheme and Reuss's scheme are tabulated by Simmons (1965). These are shown in Fig. 20. Although MgO velocities show a well-defined linear behaviour with temperature, it is very difficult to extract a single coefficient from the rock data. Average values seem to vary from about $dV/dT = -2{\cdot}5 \times 10^{-4}$ km/s/°C for basalt to -30×10^{-4} km/s/°C for dunite. For MgO the averaged results are $dV/dT = -5{\cdot}1 \times 10^{-4}$ and $-6{\cdot}9 \times 10^{-4}$ km/s/°C for the Voigt and Reuss

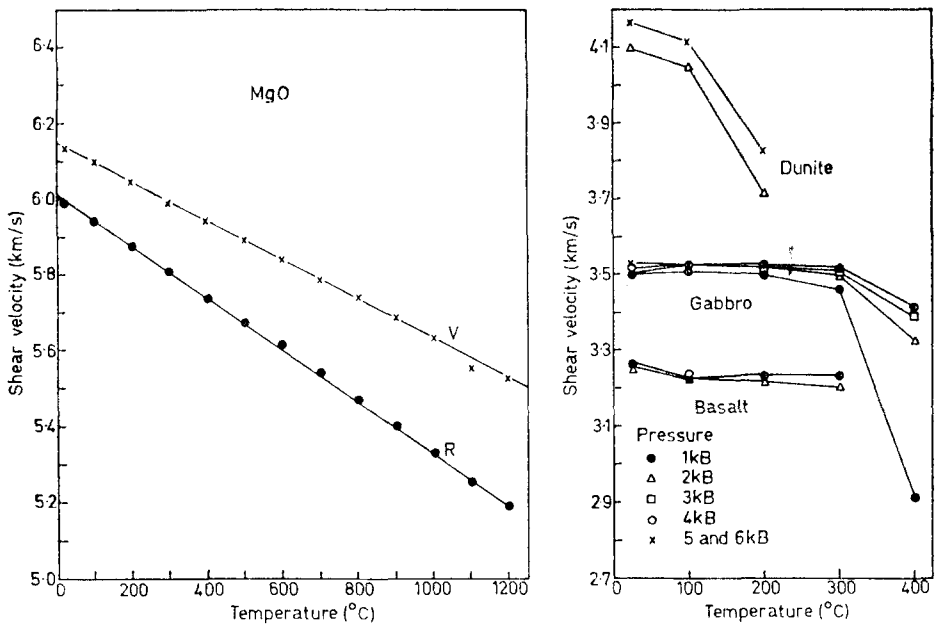

FIG. 20. Temperature dependence of the shear velocities. MgO data are from Susse (1961), 'V' and 'R' indicate averaging according to Voigt's and Reuss' schemes, respectively. Data for rocks are from Hughes & Maurette (1957).

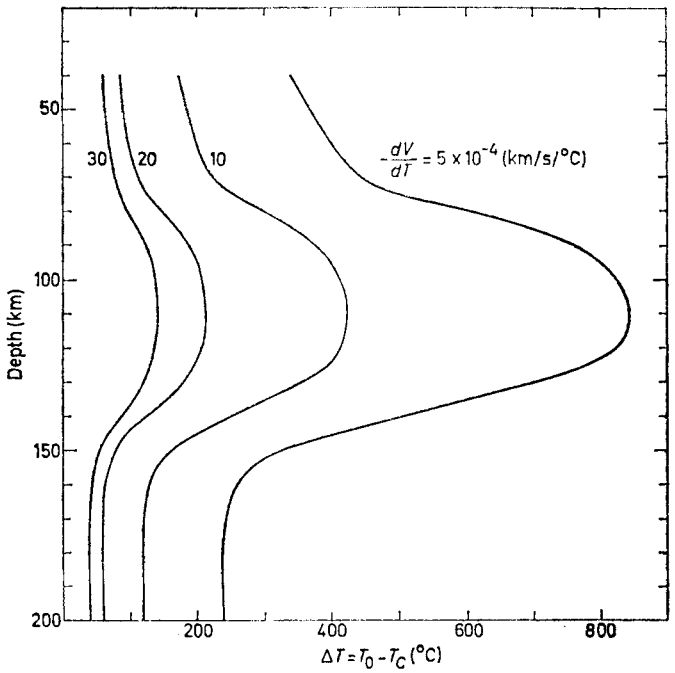

FIG. 21. Temperature differences under oceans and continents with dV/dT as a parameter. A constant value (C) can be added to or subtracted from each temperature profile.

schemes, respectively. Another determination for MgO is $-4{\cdot}8 \times 10^{-4}$ km/s/°C (Schreiber & Anderson 1966).

In the absence of well-defined results, we took four different constant values for dV/dT ($= -5$, -10, -20, and -30×10^{-4} km/s/°C) and computed temperature differences under oceans and continents as a function of depth. The results are shown in Fig. 21. For these curves, we took $C = 0$. If this is not the case, then a constant value equal to the difference should be added to the computed ΔT curves.

The results in Fig. 21 show that the maximum temperature difference under oceans and continental shields is at a depth of about 110 km. The magnitude of ΔT varies greatly with the value of chosen dV/dT, with the oceanic regions having the higher temperature. MacDonald (1963) and Clark & Ringwood (1964) obtained similar results except that their temperature differences show a less pronounced maximum. It seems clear from Fig. 21 that $-dV/dT = 5 \times 10^{-4}$ is much too low for upper mantle material.

More definite temperature results may be obtained by this method when more dV/dT data become available at high temperatures and pressures, and the velocity profiles are determined more accurately for more localized areas.

D. *Density variations in the mantle.* In this section we will consider not the radial but the lateral variations of density, i.e. we will examine deviations of the mass distribution from that of an axially symmetric body.

At the surface of the Earth, lateral variations are clear from the topographic features. It is assumed that at some depth which is a small fraction of the Earth's radius, isostatic compensation takes place, and below this, the equidensity surfaces coincide with equipotential surfaces. Gravity observations at the Earth's surface

are affected strongly by the shallow features. Correcting for these defines the isostatic anomalies.

In recent years, orbital data from artificial satellites have provided an excellent means for studying density variations. Geoid heights were computed from observations using both optical and Doppler techniques. The computational techniques as well as the results have been described by Kaula (1966), Guier & Newton (1965) and others. The observed geoid height is in general expressed in terms of spherical harmonics, and the results are estimated to be reliable up to the sixth harmonic (Kaula 1966). Differences between the observed geoid and reference spheroid vary by as much as 170 m, and the results of Guier & Newton (1965) are shown in Fig. 22.

The observed undulations of the geoid do not show any apparent correlations to general physiological features of the Earth's surface such as oceans and continents. Expansion of the surface topography of continents and ocean depths to approximately the same order harmonics as the geoid heights also confirm the lack of correlation (Slichter 1966). This means that the low order harmonic coefficients of surface features are too small to affect the coefficients of the lower harmonics obtained from satellite data.

With the elimination of the surface sources, deeper sources of density anomalies must be sought to explain the geoid undulations. Kivioja & Lewis (1966) computed the geoid undulations for surface features and isostatic compensating masses, according to the Airy–Heiskanen hypothesis. The depth of compensation was taken to be $d = 30$ km. Their results, which are partially included in Fig. 22 for maxima and minima, do not show any observable correlation with the satellite results. Wang (1965) obtained a correlation coefficient of $-0{\cdot}82$ between geoid and heat flow distribution using only second order harmonics and suggested anomaly sources within the outer 200 km of the mantle. It is not clear that his results will hold with the newest satellite data, where second order coefficients are about four times larger than the earlier values. At the present, the indications are such that the density anomalies must be at depths greater than 50 km.

The determination of the mass distribution in the mantle, given the geoid undulations, cannot be carried out uniquely. However, we can obtain a set of solutions for various depths. Taking a surface distribution and expanding it in spherical harmonics to the same order as the satellite geoid, Arkani-Hamed & Toksöz (1967) computed the mass density at various depths below the surface. In this procedure it is assumed that the geoid undulations are due to mass anomalies centred at the same radial distance from the Earth's centre. Some maximum and minimum surface densities at various depths are listed in Table 2.

Conversion of these values to actual density differences ($\Delta\rho$) requires the radial distance over which the variation ($\Delta\rho$) is to be extended. If the density variations can be fixed, then the size of the anomalous regions can be obtained. One place where this is possible is the mantle–core boundary. Taking the density difference

Table 2

Maximum and minimum values of surface density of mass at various depths

Depth of surface (km)	Mass Density (g/cm²) Maximum	Minimum
70	$8{\cdot}5\times10^{4}$	$-8{\cdot}5\times10^{4}$
400	$1{\cdot}1\times10^{5}$	$-1{\cdot}1\times10^{5}$
700	$1{\cdot}7\times10^{5}$	$-1{\cdot}7\times10^{5}$
2900	$5{\cdot}6\times10^{6}$	$-5{\cdot}6\times10^{6}$

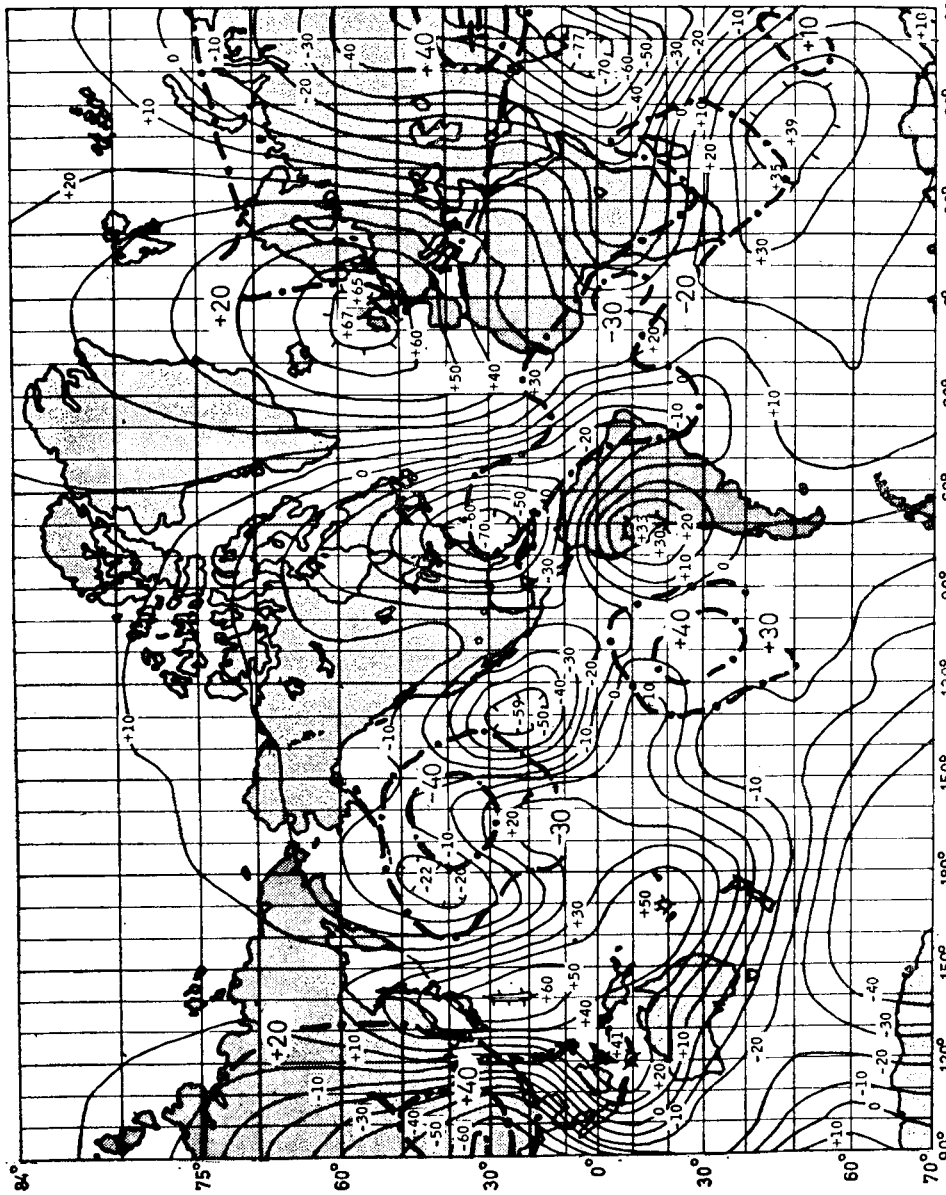

FIG. 22. Differences between the geoid determined from the Doppler observations as given by Guier & Newton (1965) and the reference spheroid. The dashed contours are the maxima and minima of the undulations computed by Kivioja & Lewis (1966) for surface features and their compensating masses according to the Airy–Heiskanen hypothesis.

$\Delta\rho = 4{\cdot}5\,\mathrm{g/cm^3}$ between the lower mantle and the core, the undulations at the mantle–core boundary can be computed. The maximum values are $+12$ and -12 km. We must remember that these values are computed on the assumption that everything else in the mantle is laterally homogeneous.

There is no question that with reasonable density variations (i.e. $\Delta\rho \approx \pm 0{\cdot}01\,\mathrm{g/cm^3}$) within the upper few hundred kilometres of the mantle, observed geoid anomalies can be accounted for. The contributions from the mantle–core boundary must be estimated from seismic data. For example, anomalies of the travel times of seismic waves reflected from the core (*PcP*) will provide a means of determining the core boundary contributions.

4. Conclusions

In this paper we have presented the seismological evidence for the presence of both vertical and lateral inhomogeneities in the Earth's mantle. Anomalous velocity behaviours or 'discontinuities' in the upper mantle at depths of 350 and 700 km were detected earlier and explained as possible phase changes. Discontinuities at depths of 1200 and 1900 km are well defined for the Japan–Kamchatka–Aleutian–Montana paths. It is not possible to state with certainty at this time whether they are global. Their presence indicates regions where there are either phase or composition changes or both. In any case, they point to departures from homogeneity in the lower mantle, in contrast to earlier beliefs.

The lateral variations in the mantle are most pronounced in the upper mantle although they seem to be present in the lower mantle, too. Our estimation of temperature differences from shear velocities under oceans and continental shields are compatible with those based strictly on heat flow and thermal data. Temperatures are between 100 and 500° C different (300° C is a good average) and are higher under the oceans than they are under continental shields at a depth of about 100 km. At shallower and greater depths this difference decreases. Tectonic areas of continents represent an intermediate stage between shields and oceans. We can define a scale of maturity for the evolution and differentiation of the crust from the upper mantle. The upper mantle under the oceans is least differentiated. It must contain more radioactive heat sources and associated lighter components to account for higher temperatures and lower velocities. Shields, on the other hand, represent regions where heat sources and acidic components are differentiated into a crust. Tectonic areas are in an in-between stage where this differentiation may still be in progress.

Geoid height studies indicate that there are density variations in the mantle somewhere deeper than 50 km. At the present time it is possible to place these variations anywhere between depths of about 100 km and the mantle–core boundary. Data from other sources are needed before the geoid heights can be interpreted uniquely.

Acknowledgments

This work was supported by the Advanced Research Projects Agency (and monitored by the Air Force Office of Scientific Research) under Contract No. AF49(638)-1632 at the Massachusetts Institute of Technology and Contract No. AF49(638)-1337 at the California Institute of Technology. The authors are grateful to Professor Francis Birch for his critical review of the manuscript and suggestions.

M.N.T.
Department of Geology and Geophysics,
Massachusetts Institute of Technology,
Cambridge, Massachusetts.

M.A.C.
Department of Geological Sciences,
Brown University,
Providence, Rhode Island.

D.L.A.
Division of Geological Sciences,
California Institute of Technology,
Pasadena, California.

References

Alexander, S. S., 1963. Crustal structure in the Western U.S. from multi-mode surface wave dispersion, Ph.D. Thesis, California Institute of Technology, Pasadena.

Alsop, L. E., 1963. Free spheroidal oscillations of the Earth at very long periods, Part I, *Bull. seism. Soc. Am.*, **53,** 483–501.

Anderson, D. L., 1964. Universal dispersion tables, 1, Love waves across oceans and continents on a spherical Earth, *Bull. seism. Soc. Am.*, **54,** 681–726.

Anderson, D. L., 1965. Recent evidence concerning the structure and composition of the Earth's mantle, *Physics and Chemistry of the Earth,* Vol. 6, pp. 1–129. Pergamon, Oxford.

Anderson, D. L., 1967. Latest information from seismic observations, Chapter III in *The Earth's Mantle.* Academic Press, New York.

Anderson, D. L. & Toksöz, M. N., 1963. Surface waves on a spherical Earth, 1, Upper mantle structure from Love waves, *J. geophys. Res.*, **68,** 3483–3500.

Archambeau, C. B., Flinn, E. A. & Lambert, D. G., 1967. Detection, analysis and interpretation of teleseismic signals—compressional phases from the Bilby, Shoal and Fallon events (summary), *Geophys. J. R. astr. Soc.*, **10,** 369–370.

Arkani-Hamed, J. & Toksöz, M. N., 1967. Satellite observations and density anomalies in the Earth's mantle, in preparation.

Asbel, I. J., Keilis-Borok, V. I. & Yanosvkaja, T. B., 1966. A technique of a joint interpretation of travel-time and amplitude–distance curves in the upper mantle studies, *Geophys. J. R. astr. Soc.*, **11,** 25–55.

Birch, F., 1952. Elasticity and constitution of the Earth's interior, *J. geophys. Res.*, **57,** 227–286.

Birch, F., 1964. Density and composition of mantle and core, *J. geophys. Res.*, **69,** 4377–4388.

Brune, J. N. & Dorman, J., 1963. Seismic waves and Earth structure in the Canadian shield, *Bull. seism. Soc. Am.*, **53,** 167–209.

Bugayevskii, G. N., 1964. Travel-time curve of seismic waves and structure of the mantle, *Izv. sib. Otdel. Akad. Nauk SSSR,* **18,** 151–168.

Bullen, K. E., 1963. *Introduction to the Theory of Seismology.* Cambridge University Press.

Carder, D. S., Gordon, D. W. & Jordan, J. N., 1966. Analysis of surface focus travel times, *Bull. seism. Soc. Am.*, **56,** 815–840.

Carder, D. S., 1964. Travel times from central Pacific nuclear explosions and inferred mantle structure, *Bull. seism. Soc. Am.*, **54,** 2271–2294.

Chinnery, M. A. & Toksöz, M. N., 1966. *P*-wave velocities in the mantle : I, below 700 km, *Bull. seism. Soc. Am.*, **56,** in press.

Clark, S. P., Jr & Ringwood, A. E., 1964. Density distribution and constitution of the mantle, *Rev. Geophys.*, **2,** 35–88.

Cleary, J. & Hales, A. L., 1966. An analysis of the travel times of *P* waves to North American stations, in the distance range 32° to 100°, *Bull. seism. Soc. Am.*, **56,** 467–489.

Dewart, G. & Toksöz, M. N., 1965. Crustal structure in East Antarctica from surface wave dispersion, *Geophys. J. R. astr. Soc.*, **10,** 127–139.

Doyle, H. A. & Webb, J. P., 1963. Travel times to Australian stations from Pacific nuclear explosions in 1958, *J. geophys. Res.*, **68,** 1115–1120.

Golenetskii, S. I. & Medvedeva, G. Y., 1965. On discontinuities of the first kind in the Earth's upper mantle, *Izv. Akad. Nauk SSSR*, Fiziki Zemli, **1,** 57–62.

Green, P. E., Jr, Frosch, R. A. & Romney, C. F., 1965. Principles of an experimental large aperture seismic array (LASA), *Proc. Instn elect. Engrs*, **53,** 1821–1833.

Guier, W. H. & Newton, R. R., 1965. The Earth's gravity field as deduced from the Doppler tracking of five satellites, *J. geophys. Res.*, **70,** 4613–4625.

Gutenberg, B., 1958. Velocity of seismic waves in the Earth's mantle, *Trans. Am. geophys. Un.*, **39,** 486–489.

Gutenberg, B., 1959. *Physics of the Earth's Interior.* Academic Press, New York.

Herrin, E., 1966. Revision of travel times for longitudinal body waves (abstract), *Trans. Am. geophys. Un.*, **47,** 168.

Hughes, D. S. & Maurette, C., 1957. Variation of elastic wave velocities in basic igneous rocks with pressure and temperature, *Geophysics*, **22,** 23–31.

Jeffreys, H. & Bullen, K. E., 1958. *Seismological Tables*, British Association for the Advancement of Science, Gray Milne Trust, London.

Johnson, L., 1966. Measurement of mantle velocities of *P* waves with a large array, Ph.D. thesis, California Institute of Technology, Pasadena.

Kaula, W. M., 1966. Tesseral harmonics of the Earth's gravitational field from camera tracking satellites, *J. geophys. Res.*, **71,** 4377–4388.

Kivioja, L. A. & Lewis, A. D. M., 1966. Free-air gravity anomalies caused by the gravitational attraction of topographic, bathymetric features and their isostatic compensating masses and corresponding geoid undulations, Gravity anomalies: Unsurveyed areas, *Am. geophys. Un. geophys. Monogr. Ser.*, No. 9, pp. 89–95.

Kosminskaya, I. P. & Riznichenko, Y. V., 1964. Seismic studies of the Earth's crust in Eurasia, Chapter 4 in *Research in Geophysics.* M.I.T. Press, Cambridge, Massachusetts.

Landisman, M., Satô, Y. & Nafe, J., 1965. Free vibrations of the Earth and the properties of its deep interior regions, Part 1: Density, *Geophys. J. R. astr. Soc.*, **9,** 439–502.

Lee, W. H. K., 1963. Heat flow data analysis, *Rev. Geophys.*, **1,** 449–479.

Lubimova, E. A., 1958. Thermal history of the Earth with consideration of the variable thermal conductivity of its mantle, *Geophys. J. R. astr. Soc.*, **1,** 115–134.

MacDonald, G. J. F., 1959. Calculations on the thermal history of the Earth, *J. geophys. Res.*, **64,** 1967–2000.

MacDonald, G. J. F., 1961. Surface heat flow from a differentiated Earth, *J. geophys. Res.*, **66,** 2489–2493.

MacDonald, G. J. F., 1963. The deep structure of continents, *Rev. Geophys.*, **1,** 587–665.

McConnell, R. K., Gupta, R. N. & Wilson, J. T., 1966. Compilation of deep crustal seismic refraction profiles, *Rev. Geophys.*, **4,** 41–100.

Niazi, M. & Anderson, D. L., 1965. Upper mantle structure of western North America from apparent velocities of *P* waves, *J. geophys. Res.*, **70,** 4640–4653.

Nuttli, O., 1963. Seismological evidence pertaining to the structure of the Earth's upper mantle, *Rev. Geophys.*, **1,** 351–400.

Pakiser, L. C. & Steinhart, J. S., 1964. Explosion studies in the western hemisphere, Chapter 5 in *Research in Geophysics*. M.I.T. Press, Cambridge, Massachusetts.

Press, F., 1964. Long-period waves and free oscillations of the Earth, Chapter 1 in *Research in Geophysics*. M.I.T. Press, Cambridge, Massachusetts.

Ringwood, A. E., 1962. Mineralogical constitution of the deep mantle, *J. geophys. Res.*, **67,** 4005–4010.

Satô, Y., 1958. Attenuation, dispersion and the wave guide of the *G* wave, *Bull. seism. Soc. Am.*, **48,** 231–251.

Schreiber, E. & Anderson, O. L., 1966. Temperature dependence of the velocity derivatives of periclase, *J. geophys. Res.*, **71,** 3007–3102.

Simmons, G., 1965. Single crystal elastic constants and calculated aggregate properties, *J. of Graduate Research Center*, **34,** 1–269. Published by Southern Methodist University, Dallas, Texas.

Slichter, L. B., 1966. A glimpse at the geophysical scene, *Trans. Am. geophys. Un.*, **47,** 346–354.

Susse, C., 1961. Measurement of the elastic constants of LiF and MgO as a function of temperature and pressure, *J. Rech. Cent. natn Rech. scient.*, **54,** 23–59.

Takeuchi, H., Dorman, J. & Saito, M., 1964. Partial derivatives of surface wave phase velocity with respect to physical parameter changes within the Earth, *J. geophys. Res.*, **69,** 3429–3442.

Toksöz, M. N. & Ben-Menahem, A., 1963. Velocities of mantle Love and Rayleigh waves over multiple paths, *Bull. seism. Soc. Am.*, **53,** 741–764.

Toksöz, M. N. & Anderson, D. L., 1966. Phase velocities of long-period surface waves and structure of the upper mantle, 1, Great-circle Love and Rayleigh wave data, *J. geophys. Res.*, **71,** 1649–1658.

Toksöz, M. N. & Folinsbee, R. A., 1965. Crust and upper mantle structure under island arcs, *Trans. Am. geophys. Un.*, **47,** 489.

Vvedenskaya, A. V. & Balakina, L. M., 1959. Double refraction in the Earth's mantle, *Izv. Akad. Nauk SSSR, Ser. Geofiz.*, **7,** 1138–1146.

Wang, C., 1965. Some geophysical implications from gravity and heat flow data, *J. geophys. Res.*, **70,** 5629–5634.